ELSEVIER

Journal of Fluids and Structures 21 (2005) 335–361

JOURNAL OF FLUIDS AND STRUCTURES

www.elsevier.com/locate/jfs

Experimental investigation of vortex-induced vibration of long marine risers

A.D. Trim[a,*], H. Braaten[b], H. Lie[b], M.A. Tognarelli[c]

[a]*BP Exploration, Chertsey Road, Sunbury on Thames, TW16 7LN, UK*
[b]*Marintek–Department of Offshore Structures, P.O. Box 4125, Valentinlyst, NO-7450, Trondheim, Norway*
[c]*ExxonMobil Upstream Research Company, URC-GW3-774A, P.O. Box 2189, Houston, TX 77252, USA*

Received 6 October 2004; accepted 14 July 2005
Available online 28 September 2005

Abstract

There is considerable disparity between predictions of marine riser vortex-induced vibration (VIV) fatigue damage, and often the agreement between computer models and observed VIV-related damage is inaccurate by orders of magnitude. Resulting problems for deepwater riser design are the need for large safety factors on fatigue damage predictions and the use of expensive vortex-suppression devices (e.g. helical strakes). Understanding is especially limited for long risers, which may be excited in multiple and higher modes. Norwegian Deepwater Programme (NDP)—a group of oilfield licensees in Norway—has commissioned experiments on riser models over a range of scales and current conditions in order to improve the ability to predict VIV. Recently, testing of a model with an L/D (length-to-diameter ratio) of 1400 was conducted at Marintek's Ocean Basin in Trondheim. The riser was tested without VIV suppression and with various strake arrangements. Testing was performed on an innovative test rig that could simulate uniform and linearly sheared currents, with a composite fibre model that featured a dense array of high-quality instrumentation. In-line and cross-flow responses were considered important with respect to fatigue. Indeed, this study reinforces recently published results that in-line fatigue damage is as severe as cross-flow fatigue damage. However, industry analysis approaches generally ignore in-line damage due to VIV. The findings also indicate that the response character of a bare riser can be quite distinct from that of a riser partially or fully covered with helical strakes. In addition, while helical strakes of different types can be effective in mitigating VIV fatigue of long risers, their performance is dependent on their geometry. Finally, the results suggest that a key consideration in VIV fatigue design is the length of suppression coverage and the nature of the flow to which the bare section of the riser is exposed.

1. Introduction

Observations of marine riser response show current-induced vortex-induced vibration (VIV) to be a widely occurring phenomenon, with the potential to cause costly and environmentally damaging fatigue failures. In the deep waters of the Gulf of Mexico, West Africa and Norway, for example, where oil and gas exploration and production continue apace, VIV may account for the greatest contribution to overall riser fatigue damage. Wave- and vessel motion-related damage may stay roughly the same, or diminish as water depth increases, but currents can act over the full water depth,

*Corresponding author. Tel.: +44 1225 461256.
E-mail address: andytrim@adtltd.fsnet.co.uk (A.D. Trim).

0889-9746/$ - see front matter © 2005 Elsevier Ltd. All rights reserved.
doi:10.1016/j.jfluidstructs.2005.07.014

tending to make VIV more important in deeper water. This, and the fact that VIV of long risers is generally less well understood than other load effects, has led to an intensification of research activity in recent years.

Attempts to quantify VIV in general and riser VIV in particular go back a long way, but only in the last decade or so have serious efforts been made to conduct suitable experiments and establish advanced analysis tools for the assessment of long riser VIV in rather general current conditions. A review of related literature is well beyond the scope of this paper, but the interested reader is directed to: Vandiver (1993), Vandiver et al. (1996), Lie et al. (1997), Herfjord et al. (1999), Willden and Graham (2001), Tognarelli et al. (2004), Frank et al. (2004), Lie and Kaasen (2005) and Baarholm et al. (2005). Riser VIV has also been the subject of several proprietary studies by oil companies and joint industry projects (JIPs) like Norwegian Deepwater Programme (NDP).

In 2002–03 NDP commissioned a number of reviews and analyses of data held in the public-domain and by itself to assess the state of the art in VIV testing in general and high-mode, flexible cylinder response, in particular. With this background, NDP commissioned high-mode VIV testing of long risers with and without vibration suppression devices. There were three objectives:

(i) acquire data to improve understanding of high-mode VIV of long risers in different current profiles;
(ii) provide benchmark information for calibration and validation of codes that predict riser response; and
(iii) assess suppression effectiveness of strakes with different geometries and different percentage coverages over the riser length.

This paper will cover the results that pertain to these objectives.

It was recognized that achievement of field-scale Reynolds number together with high L/D was impossible in an indoor laboratory. This was accepted as a necessary limitation and high L/D was given priority.

The Norwegian Marine Technology Research Institute (Marintek) performed the testing in late 2003 at their Trondheim Ocean Basin facility using a 38 m long riser model. A summary of the review work preceding these experiments and a brief presentation of the model test programme can be found in Trim et al. (2004). Tognarelli et al. (2004) and Frank et al. (2004) report earlier tests on a densely instrumented 10 m model in Marintek's rotating rig facility. Those studies demonstrated high-mode structural response for a long riser without suppression, generally according to expected trends, but with some new findings in linearly sheared flow (the dominant frequency of the in-line response was lower than expected and relatively insensitive to current speed). They also showed that 16 diameter pitch strakes with a height of 0.25 diameter effectively mitigated VIV and fundamentally changed the riser response when fully covering the riser. However, in partial coverage tests the strakes were not as effective. The current set of experiments draws even more closely to the full-scale situation in a structural sense, in that more modes participate in the response and the dynamics are tension-dominated throughout the range of excitation, as they would be for a riser in field application. The tests are still, however, at low Reynolds number (maximum circa 70 000), whereas field conditions include low and high Reynolds number regimes. For a full-scale riser diameter of (say) 0.5 m and ocean currents of up to 2 m/s, Reynolds numbers approaching a million may apply, embracing three flow regimes: subcritical, critical and supercritical. The scale effect between the present tests and full-scale may therefore be substantial, but it was beyond the scope of this work to consider these effects. The present experiments also introduce a second strake geometry whose pitch is 5 diameters with a height of 0.14 diameters. If such a geometry could mitigate VIV fatigue, its more compact height might reduce in-line drag force on the riser. Finally, careful attention is paid to the necessary gaps in suppression coverage and their influence on performance. This paper is an extension of Trim et al. (2004), highlighting the following key findings from the data:

(i) bare riser response follows expected trends;
(ii) though ignored in analysis codes, in-line fatigue damage is as severe as cross-flow fatigue damage;
(iii) triple-start helical strakes are effective in mitigating VIV fatigue damage when fully covering the riser;
(iv) practical limitations on full strake coverage, like cut-outs for banding, do not significantly reduce strake performance;
(v) a 17.5D pitch/0.25D height strake design is, in the context of this experiment, more effective in VIV mitigation than a 5D pitch/0.14D height design; this can affect fatigue damage by orders of magnitude;
(vi) lower drag (compared to 17.5D pitch/0.25D height strakes) from the 5D pitch/0.14D height geometry might be offset by higher motion, but measurements have not confirmed this; and
(vii) strake performance deteriorates as coverage is reduced, particularly in uniform flow.

The notation 17.5/0.25 and 5.0/0.14 is used to refer to strakes with 17.5D pitch and 0.25D height and to strakes with 5.0D pitch and 0.14D height, respectively.

2. Experimental set-up

The goals of these tests were to use a dense instrumentation grid: (i) to investigate the local and global behaviour of a model whose dynamics were tension-dominated and that would respond in high modes without VIV suppression devices; (ii) to assess the effectiveness of different types of helical strake, covering different proportions of the length of the model. This section describes the rig, model and instrumentation that were utilized to achieve these objectives.

2.1. Rig

A key challenge in the rig design was to limit rig-riser interaction over the entire frequency range associated with riser VIV bending response. This frequency range was estimated to be 2–30 Hz. This constraint on rig-riser interaction was achieved via an innovative mass-dominated test rig, with natural frequencies well below the lowest riser bending frequency.

A design loop was executed in order to achieve a test set-up that met several design criteria. Among the key considerations were:

(a) the system should have sufficient strength for safety and reliability,
(b) eigenfrequencies for the rig should be no more than $\frac{1}{2}$ of the first riser bending eigenfrequency, to avoid contaminating interactions,
(c) torsional rotation should be limited so that cross-flow (CF)/in-line (IL) orientation is not significantly altered,
(d) excessive riser deflections due to drag force should be avoided so that the desired current profile is preserved as nearly as possible,
(e) the rig should have the ability to accommodate set-down due to drag or gravity, and
(f) the rig and model should be easy to install and operate.

This led to a test rig that consisted of the following (see Fig. 1).

(i) A 38 m long horizontal riser model attached to the test rig via universal joints. The riser could bend IL and CF, but was constrained in torsion relative to the rest of the rig.
(ii) Clump weights, 520 kg each, at the riser ends. The clump weights act in tandem with pendulum arms to moderate tension variation in the riser; the tension ranged approximately between 4 and 6 kN over the full set of test speeds. Their large mass keeps pendulum modes of the rig in the low-frequency range, away from riser bending frequencies. One of the clump weights included a heave compensator to smoothly accommodate riser set-down due to drag and to control the stiffness and eigenfrequency of the rig mode in the riser axial direction. The heave compensator consisted of two sets of springs in parallel.
(iii) Inclined pendulum arms connecting each clump weight to the gondola/crane via vertical springs. The springs maintain a compliant connection between the clump weights and the gondola/crane. The pendulum arms limited the rotation of the clump weights due to steady IL drag on the riser. The horizontal component of the force on the pendulum arms due to the clump weights provided the riser tension. As the riser 'set down' during testing, some static roll motion of the clump weights occurred as sketched in the top of Fig. 1. However, universal joints at each riser end prevented this rotation from being transferred to the riser. The pendulum arms were connected to the clump weights via triangular frame units, making it possible to disconnect the clump weights from the rest of the test rig during model changes and during tests in linearly sheared flow, where one end of the riser remained stationary.
(iv) A horizontal support framework with springs connected to the rig in the tow direction to maintain a compliant connection without introducing rig-riser interference.

Two current profiles were generated: uniform and linearly sheared. This is illustrated in Fig. 2. Uniform current was simulated by towing the rig in one direction using the crane. Linearly sheared current was simulated by fixing one end of the riser and using the crane and gondola in tandem to traverse a circular arc.

For the model tests with linearly sheared flow, the complete test rig at the gondola end of the test set-up could rotate in order to maintain clump weight orientation relative to the riser as it traversed the arc. The arc motion was computer-controlled with an accuracy of 2–3 cm. This accuracy was found to be sufficient with respect to tension variation because of the compliant behaviour of the inclined pendulum/clump weight system and with respect to the sheared

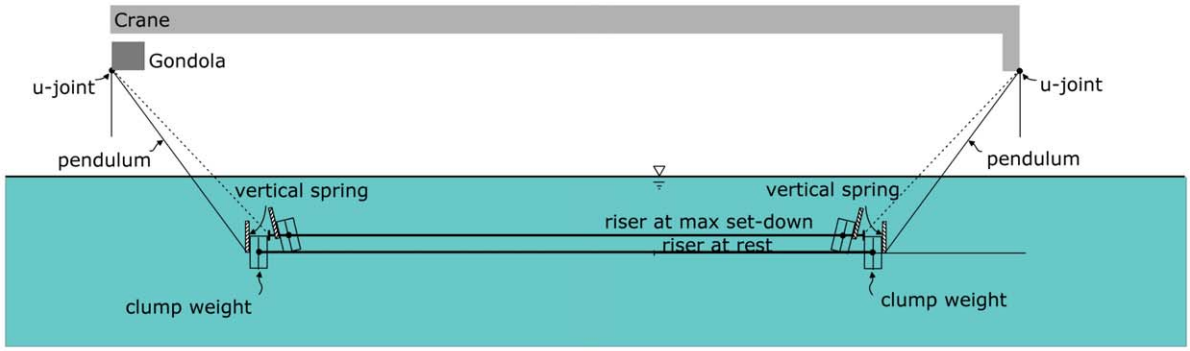

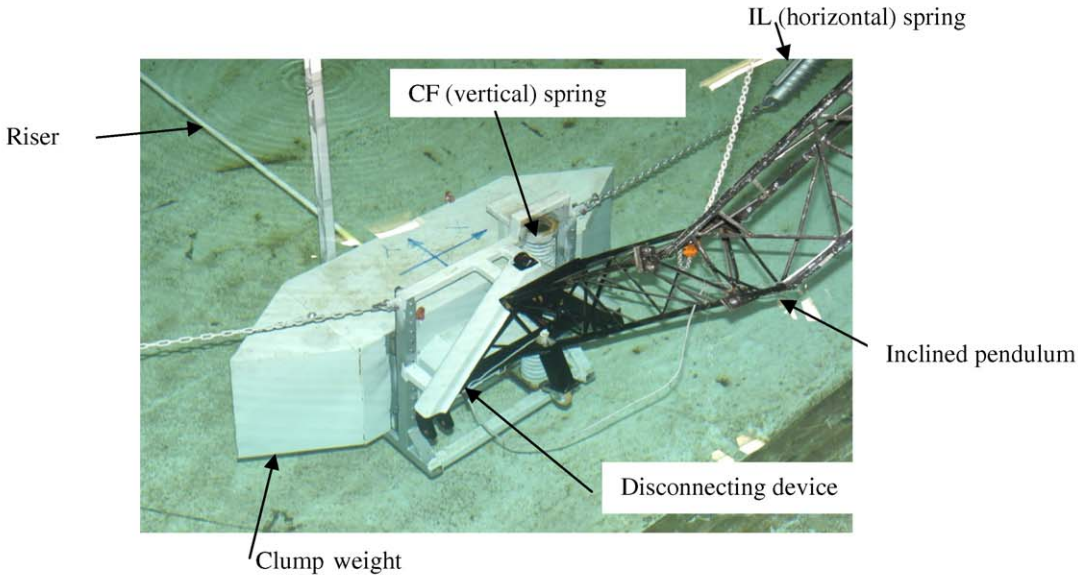

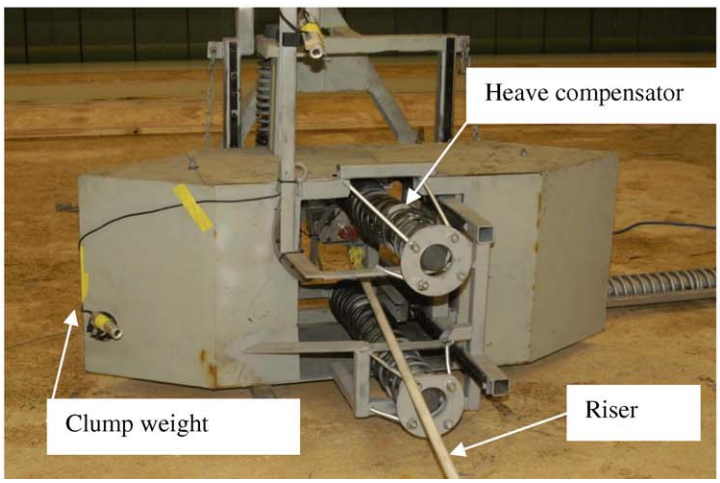

Fig. 1. Test set-up. Upper: schematic of test rig used for VIV model test (vertical view). Middle and lower: photos of clump weights and heave compensator.

velocity. The standard deviation of the tangential tow speed was a maximum of 0.4% of the mean speed. The rotation of the test rig was controlled by two wires in a V-shape between the horizontal arms at the gondola end and the centre of rotation at the fixed end.

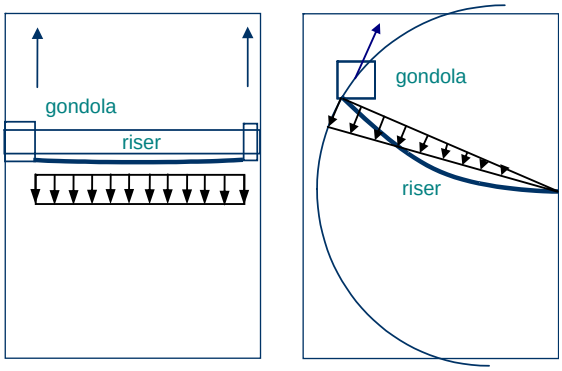

Fig. 2. Test schematics (plan view). Left: uniform flow; right; linearly sheared flow.

2.2. Riser model

The (bare) riser model was a 27 mm diameter reinforced fibreglass pipe with a wall thickness of 3 mm, specially made for these tests. The model dimensions reflect a careful compromise between high-mode response and instrumentation density. The available internal space of the riser model together with the diameter of the instrument cables limited the amount of instrumentation that could be used. Thus, from the viewpoint of maximizing the instrumentation grid density, a larger diameter pipe would have been preferred. However, the increased bending stiffness would have called for higher tow velocities than could be achieved, in order to excite the desired high modes. Additionally, the stiffness of real deepwater risers is typically tension-dominated. To reflect this as nearly as possible, a goal was to keep bending stiffness and hence model diameter relatively low.

Since the riser instrumentation—strain gauges and accelerometers—was attached to the outside of the pipe, the apparent riser diameter was slightly larger at instrumented sections. A coating was applied to seal and smooth these protuberances. Fig. 3 shows a picture of the coated instrumentation on the riser. The riser model was flooded with water, and the mass ratio, including instrumentation, was approximately 1.6. The mass ratio is the ratio of the mass per unit length of the riser and its contents to that of the displaced water. A value of 1.6 is in the range of mass ratios of field-scale risers.

Since the riser model was comprised of a composite material with uncertain stiffness, strength and fatigue properties, several property verification tests were performed. First, a section of pipe was fatigue tested. Approximately 1.2 million oscillations were run and no damage was seen. The stiffness properties of the pipe were measured before, during and after the fatigue tests, and they remained constant. The Young's modulus was found to be $36.2 \times 10^9\,\mathrm{N/m^2}$. A strength test was also performed. The sample pipe included all assumed weak sections; i.e. end terminations, a connection sleeve between two pipes, and an instrumentation location. The test showed that the sample pipe had a capacity of at least 10 times the pre-tension used in the tests.

2.3. Strakes

Two types of triple-start helical strake for VIV-suppression were tested. Fig. 4 shows photographs of these. The strakes were detailed scale models of prototypes with two combinations of pitch/diameter ratio, height/diameter ratio: 5.0/0.14 and 17.5/0.25. Whilst a more extensive and systematic assessment in which pitch and height were varied independently might be preferred from a scientific viewpoint, such an investigation was beyond the scope of the test programme. These geometries correspond to types commonly used within the offshore industry. The strakes were moulded with a central sleeve, which increased the pipe diameter to 33 mm. The strake height is expressed in terms of this diameter. Bending stiffness of the strakes was estimated to be about the same as that of the riser. Since the eigenfrequencies of the responding modes were dominated by the tension component of stiffness, the increased bending stiffness from strakes was assumed to have negligible effect on the modal frequencies.

Strake geometries were tested with 91%, 82%, 62% and 41% coverage over the length of the riser, as well as the bare riser. Because of the instrumentation it was impossible to cover 100% of the riser with strakes. The 91% coverage case represents the situation in which the entire length of the riser with the exception of instrument locations was covered. A typical cut-out section is shown in the bottom of Fig. 4. The 82% coverage case was of particular practical interest, as it

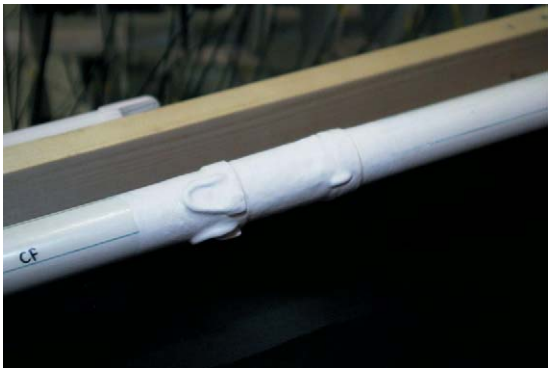

Fig. 3. Accelerometers and strain gauges mounted on riser model.

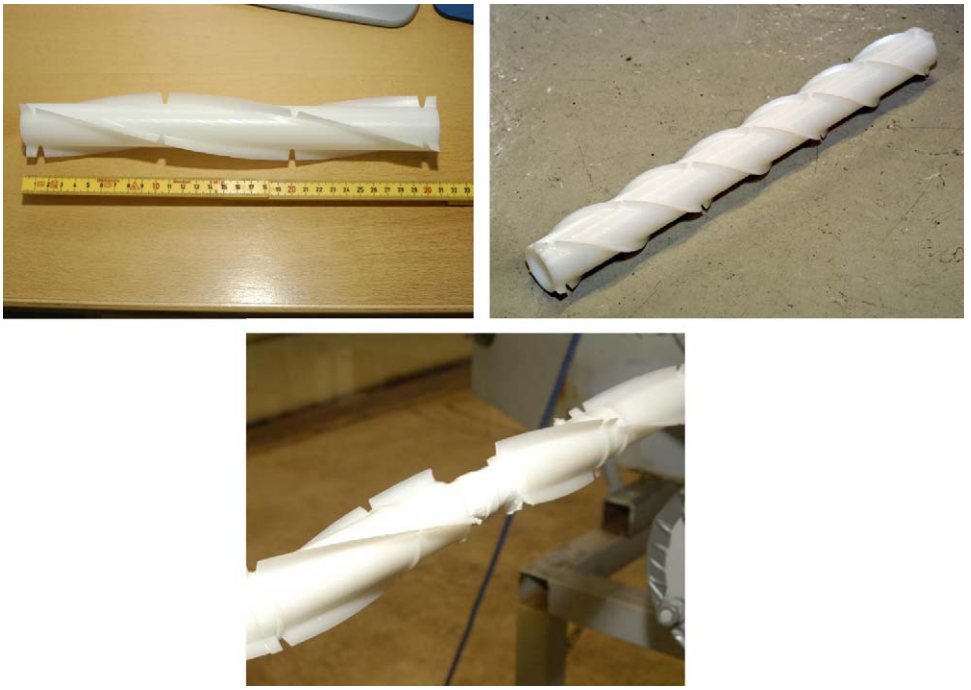

Fig. 4. Top left: example of 17.5/0.25 strake device. Top right: example of 5.0/0.14 strake device. Bottom: cut-out in strakes to accommodate instrumentation.

represented a nominal 100% coverage with cut-outs for installation banding and gaps at riser joint welds. For 91% and 82% strake coverage the distribution of strakes is uniform along the riser. For 62% and 41% coverage the strakes were removed from the riser model such that the highest current region remained covered during the linear shear flow tests. The 62% coverage scenario represents the case in which nominally the upper (high-current) 75% of the riser length is covered with strakes and there is a 13% loss of coverage due to gaps. Likewise, the 41% coverage represents a case in which the upper 50% of the riser length is nominally covered with strakes.

2.4. Instrumentation

A total of 24 CF and 40 IL strain gauges and 8 CF and 8 IL accelerometers were utilized, creating one of the most detailed instrumentation arrays to date for measuring riser VIV response. Key considerations in selecting

instrumentation were the need to have a direct measurement of strain and enough resolution to identify high bending modes in the aggregate response. The strain gauges were not uniformly spaced as in many earlier experiments. Uneven spacing of instruments reduces redundancy where symmetric or anti-symmetric modes respond and generally may help identify higher curvatures and corresponding higher mode participation.

The instrumentation also included accelerometers at clump weights, riser end-force transducers, tachometers for speed measurements, and video recordings.

For quality assurance during the test programme, rigorous calibration and verification of the instrumentation and data acquisition system were performed. This included component- and system-level checks of sensors, filters, amplifiers and analogue-to-digital (A/D) converters. Checks ranged from bench-testing to verify calibration and dynamic range to in-air static and dynamic tests to verify gain and sensor polarity. The calibration of the transducers for measuring bending strains, accelerations and forces was found to be accurate within $+/-1-2\%$ through use of an ambitious sensor-error-budget approach.

3. Data analysis

The critical consequence of VIV for riser design is fatigue damage. Thus, fatigue calculations were performed using the direct measurements of strain for all tests. In addition, to assess and improve analysis programs for predicting VIV fatigue damage, it is important to understand as nearly as possible the underlying physics of the VIV phenomenon. Some key considerations are: the amplitude of response; the frequency content of the response and its variation with flow speed; the character of the structural response (whether or not it responds in structural modes); and the influence on the response of VIV mitigation devices. To address these issues, several other analyses were performed in addition to fatigue calculations. Both IL and CF response data have been extensively analysed by a number of different techniques. Results from some of these analyses will be presented in the next section. In the present section, we give a summary of these analyses.

3.1. Modal analysis

A modal analysis technique has been used to study modal participation under different test conditions. Modal analysis has been applied previously to analyse data from other long riser VIV tests; e.g. Kaasen et al. (2000), who used rotation-rates and accelerations as input signals, and Lie and Kaasen (2005), who used strain signals. For the present work, the original intent was to use only the measured strains in the modal analysis. Accelerations were measured at a subset of locations, primarily so that they could be double-integrated in time and compared to displacement time series reconstructed from the modal analysis.

However, early in the programme development, it was decided to investigate a modal analysis approach using a combination of strain and acceleration signals as input. This approach was found to yield excellent results and was used in the final processing of data presented here. A discussion of this approach follows.

The modal decomposition is based on the assumption that the shape of the riser may be expressed as a sum of eigenmodes, or eigenfunctions, at any instant in time. The CF and IL displacements are decomposed separately; e.g. for CF displacements (x-direction), we get

$$x(z,t) = \sum_{n=0}^{\infty} w_n(t)\varphi_n(z), \tag{1}$$

where z denotes the position along the riser with origin at the "top" end, $w_n(t)$ are the modal weights, and $\phi_n(z)$ are the eigenmodes.

The relation

$$\kappa = \varepsilon/R, \tag{2}$$

where R is the riser outer radius, converts strain ε to curvature κ, which is approximately equal to the second derivative in the spatial direction. Using (1) with only a finite number of modes N, the curvature and accelerations become, in terms of eigenmode expansion,

$$\kappa(z,t) = \sum_{n=1}^{N} w_n(t)\varphi_n''(z), \quad a(z,t) = \sum_{n=1}^{N} \ddot{w}_n(t)\varphi_n(z), \tag{3}$$

where the second spatial derivative is denoted $\kappa = x''$, and the second time derivative is denoted $a = \ddot{x}$. Now, information about curvature and accelerations is only acquired for a finite number of spatial locations, $z = z_i$ with $i = 1, 2, \ldots, M$. In our case, for accelerations, $M_a^{\mathrm{IL,CF}} = 8$, and for curvature, $M_\kappa^{\mathrm{IL}} = 40$, $M_\kappa^{\mathrm{CF}} = 24$ or 23. This reflects the fact that one of the original 24 sensors failed during some of the tests. For a given instant in time, we then have $M = M_\kappa + M_a$ equations with N unknowns. We require that $N \leqslant M$ in order to avoid an under-determined system of equations. For $N = M$ the system of equations has a single, unique solution. For $N < M$ the system may be solved using the least squares method.

It is convenient to pose the system in the frequency domain when solving for curvature and accelerations simultaneously. Denoting the Fourier transform in time by a hat, $\hat{y} = F\{y\}$, we get

$$\hat{\kappa}(z,\omega) = \sum_{n=1}^{N} \hat{w}_n(\omega)\varphi_n''(z), \quad \hat{a}(z,\omega) = -\omega^2 \sum_{n=1}^{N} \hat{w}_n(\omega)\varphi_n(z), \tag{4}$$

where we have used the relationship $\hat{\ddot{y}} = -\omega^2 \hat{y}$.

The system may be posed in terms of a linear system

$$\boldsymbol{A}\hat{\boldsymbol{w}} = \hat{\boldsymbol{b}}, \tag{5}$$

where the system matrix, $\boldsymbol{A}$, contains the discrete eigenvectors and the right hand side, $\boldsymbol{b}$, contains the measurements. In detail the matrix and vectors become

$$\boldsymbol{A} = \begin{bmatrix} \varphi''^1_1 & \varphi''^1_2 & \cdots & \varphi''^1_N \\ \varphi''^2_1 & \cdot & & \cdot \\ \vdots & \cdot & \cdot & \cdot \\ \varphi''^{M_\kappa}_1 & \varphi''^{M_\kappa}_2 & \cdots & \varphi''^{M_\kappa}_N \\ \varphi^1_1 & \varphi^1_2 & \cdots & \varphi^1_N \\ \varphi^2_1 & \cdot & & \cdot \\ \vdots & \cdot & \cdot & \cdot \\ \varphi^{M_a}_1 & \varphi^{M_a}_2 & \cdots & \varphi^{M_a}_N \end{bmatrix}, \quad \hat{\boldsymbol{w}} = \begin{bmatrix} \hat{w}_1 \\ \hat{w}_2 \\ \vdots \\ \hat{w}_N \end{bmatrix}, \quad \hat{\boldsymbol{b}} = \begin{bmatrix} \hat{\kappa}_1 \\ \hat{\kappa}_2 \\ \vdots \\ \hat{\kappa}_{M_\kappa} \\ -\hat{a}_1/\omega^2 \\ -\hat{a}_2/\omega^2 \\ \vdots \\ -\hat{a}_{M_a}/\omega^2 \end{bmatrix}, \tag{6}$$

where $\varphi_n^i = \varphi_n(z_i)$.

Since the riser is oriented in the horizontal plane, the tension is constant along the riser, and sinusoids were therefore chosen as basis eigenmodes in the present analysis. The eigenmodes are therefore linearly independent. The second derivative of the eigenmodes is

$$\varphi_n(z) = \sin(n\pi z/L) \Rightarrow \varphi_n''(z) = -(n\pi/L)^2 \sin(n\pi z/L). \tag{7}$$

Having chosen linearly independent eigenmodes, the system described by (5) above is invertible, and a solution exists:

$$\hat{\boldsymbol{w}} = \boldsymbol{A}^{-1}\hat{\boldsymbol{b}}. \tag{8}$$

If it can be argued that fewer than M mode shapes participate significantly in the riser motion, the system of equations can be solved in the least squares sense. In this case the estimate of modal weights becomes

$$\hat{\boldsymbol{w}}(\omega) = (\boldsymbol{A}^{\mathrm{T}}\boldsymbol{A})^{-1}\boldsymbol{A}^{\mathrm{T}}\hat{\boldsymbol{b}}(\omega) = \boldsymbol{H}\hat{\boldsymbol{b}}(\omega). \tag{9}$$

When the number of mode shapes is M, $\boldsymbol{H} = \boldsymbol{A}^{-1}$, and the expression reduces to (8). Hence, (9) can be regarded as the general form of the estimator and (8) a special case.

The linear system in (8) and (9) is made loosely disconnected for some cases. This is done in order to try to control the noise effect from strain signals for low modes. The noise effect is discussed in more detail by Lie and Kaasen (2005). A modified system matrix $\boldsymbol{A}$, here denoted by $\tilde{\boldsymbol{A}}$, is used to find the modal weights from mode number n to mode number

N and is given by

$$\tilde{\boldsymbol{A}} = \begin{bmatrix} \begin{bmatrix} 0 \end{bmatrix} & \begin{bmatrix} \varphi''_{n+N_0} & \cdots & \varphi''_N \end{bmatrix} \\ \begin{bmatrix} \varphi_n & \cdots & \varphi_N \end{bmatrix} & \end{bmatrix}, \tag{10}$$

where the zero sub-matrix has dimensions $M_\kappa \times N_0$ and where typically $N_0 \ll N - n + 1$. In practice, the zero sub-matrix imply that only acceleration signals are used to solve for the participating modes for the N_0 lowest modes. For cases where low modes are expected to participate this technique is found to provide an improved modal analysis.

The system is solved in the frequency domain. The time-varying modal weight vector is obtained by inverse Fourier transform, $\boldsymbol{w}(t) = F^{-1}\{\hat{\boldsymbol{w}}(\omega)\}$.

The estimator (9) can be applied to CF and IL motions separately, with the matrix $\boldsymbol{H}$ constructed appropriately for the situation, depending on how many and which mode shapes are to be included.

3.2. Dominant mode with respect to displacement

From the modal analysis the modal weight standard deviations, $w_{j,SD}$ are computed, and the value of j with the largest $w_{j,SD}$ is called the dominant mode with respect to displacement.

3.3. Dominant mode with respect to curvature

The expression $(j\pi/L)^2\, w_{j,SD}$ is denoted the modal curvature standard deviation in mode j, and the value of j with the largest modal curvature standard deviation is called the dominant mode with respect to curvature. This will normally be higher than the dominant mode with respect to displacement and can be used to identify the modes that are most important for fatigue damage.

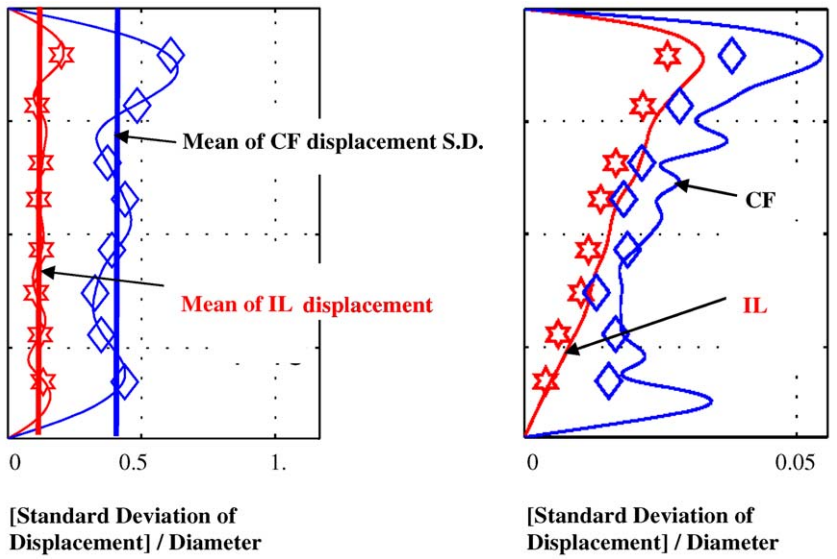

Fig. 5. Examples of displacement standard deviation along riser. Left: bare riser in uniform flow of 0.4 m/s. Right: 91% coverage of 17.5/0.25 strakes in sheared flow. Hexagrams and diamonds represent displacement standard deviation IL and CF respectively, obtained by integration of acceleration signals. Solid lines represent displacement standard deviation computed by modal analysis.

3.4. Dominant frequency

Another key parameter is the dominant frequency of response and its variation with flow speed. In the present paper, we present the frequency associated with the peak of the power spectral density of the dominant mode with respect to displacement.

3.5. Fatigue analysis

Applying the Miner summation, the fatigue damage at a specific location along the length of the riser is given by

$$D = \sum_{i=1}^{N_{\text{seg}}} \frac{n_i}{N_i} = \frac{1}{a} \sum_{i=1}^{N_{\text{seg}}} n_i (\Delta\sigma_i)^m, \tag{11}$$

where N_i is the number of cycles to failure and n_i is the number of stress cycles at stress range $\Delta\sigma_i$. Since stress is linearly proportional to strain, it is advantageous that in these tests, strain has been measured directly and need not be derived from another quantity. N_{seg} is the number of stress ranges. The number of stress cycles n_i is found via rainflow counting. The parameters a and m are typically associated with a stress range versus cycles to failure ($S-N$) curve appropriate to the material under consideration, and can be found in various fatigue design codes. In this paper we use the D curve, NORSOK standard (1998), with $\log a = 11.687$ and $m = 3.0$. Use of similar curves with $m = 3$ would just introduce a scale difference in the estimated fatigue damage.

In this paper only IL and CF fatigue damage is reported; i.e. the damage at 90° intervals around the riser periphery. Higher damage at intermediate locations can occur, but is unlikely to exceed IL and CF damage by very much under any circumstances. Other work (Baarholm et al., 2005; Tognarelli et al., 2004) shows that the maximum of IL and CF damage is normally a good indicator of maximum damage anywhere.

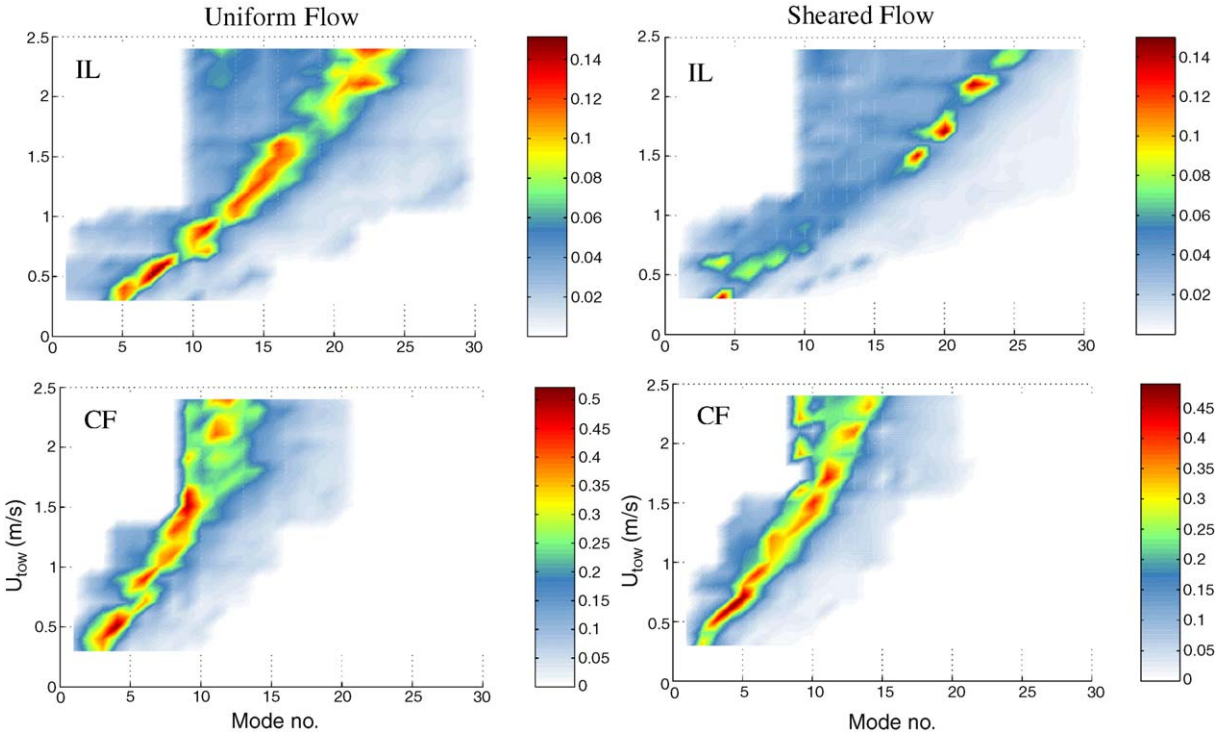

Fig. 6. Contour plots of modal weight standard deviations for bare riser.

4. Results

The test programme consisted of 341 runs and covered tow speeds from 0.3 to 2.4 m/s. It included uniform and linearly sheared current profiles. Based on preliminary calculations, CF modes between 2 and 14 were expected to be excited in this flow speed range.

The riser response varied distinctly depending on the length of strake coverage. Accordingly, the results have been divided into three groups:

(i) bare riser;
(ii) fully straked riser (91% and 82% coverage); and
(iii) partially straked riser (62% and 41% coverage).

Within each group, the riser response was observed to follow broadly similar trends.

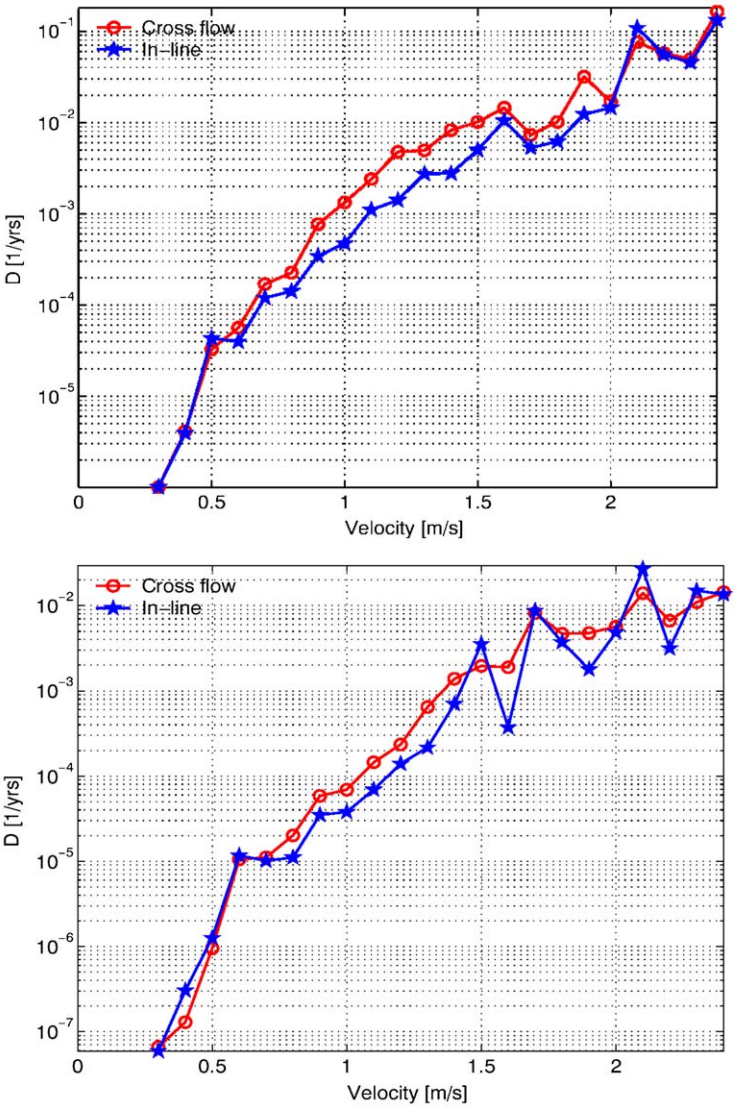

Fig. 7. CF and IL fatigue versus tow speed for bare riser. Top: uniform flow. Bottom: sheared flow.

For convenience, key summary results are grouped together in Figs. 16–20 at the end of the paper and are referred to throughout the remainder of the text, as necessary. They show results from all tests and each figure consists of several subplots presenting results against tow speed. The subplots are referred to in the following discussion by their row (r) and column (c) numbers. These figures present (spatial) mean and maximum of (temporal) displacement standard deviation over the riser, peak frequency of the dominant mode with respect to displacement, and the dominant modes for displacement and curvature. The displacement standard deviation is normalized by the diameter of the bare riser. The displacement has been reconstructed using the results of the modal analysis. Since the mean is obtained by averaging all the temporal standard deviations at locations along the riser, this metric is subject to the density of the measurement grid. Various additional aspects of behaviour are discussed sequentially below, and are illustrated in Figs. 5–15.

Fig. 5, left, shows an example of displacement standard deviation along the riser together with its mean. The maximum is taken as the largest among all of the standard deviations collected along the length. In order to get accurate

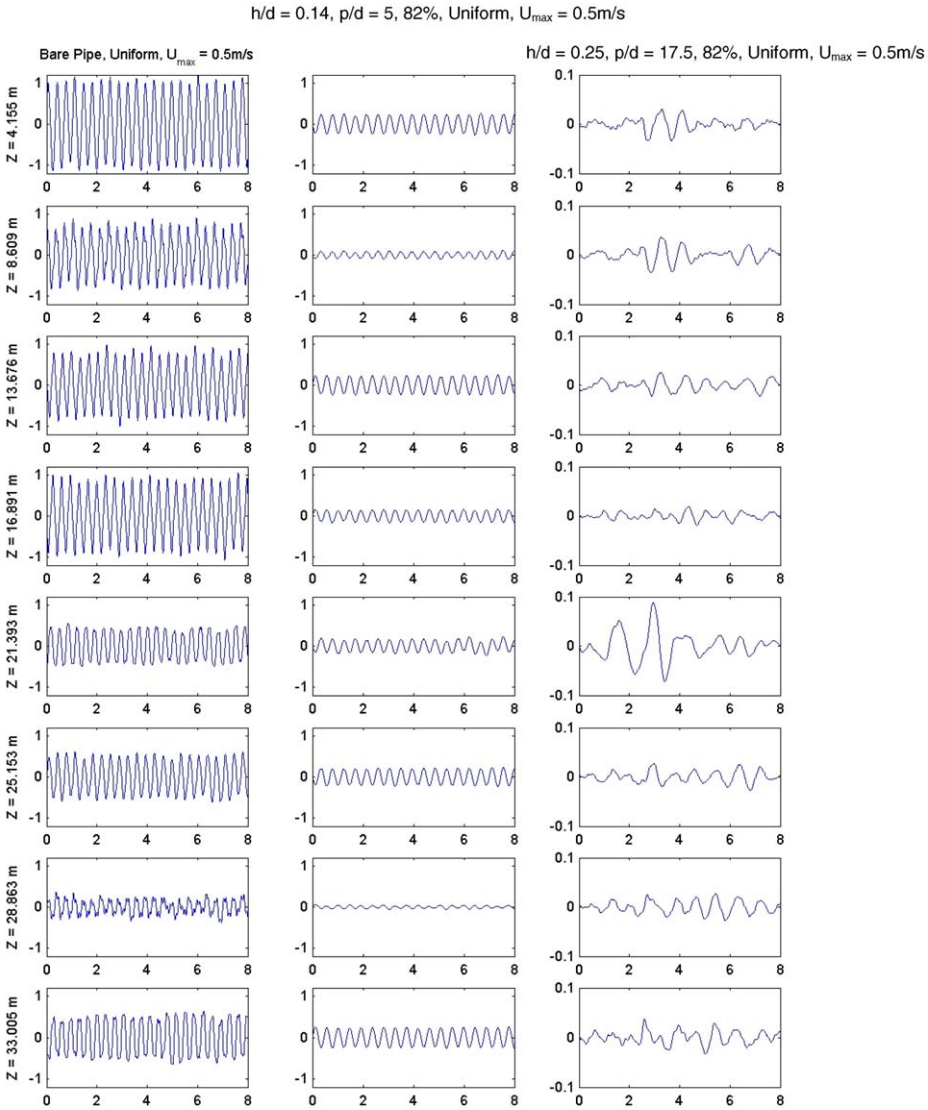

Fig. 8. Time histories of CF displacement/diameter at different stations, Z, along riser in uniform flow. 0.5 m/s. Left column: bare riser. Centre column: 82% coverage of 5.0/0.14 strakes. Right column: 82% coverage of 17.5/0.25 strakes. Plots in right column magnified for clarity.

results from the modal analysis, the participating mode numbers used as input to the analysis were tuned on a trial and error basis. The results are in some cases sensitive to the participating mode numbers, but are considered in general to be reasonably accurate. However, for some cases it was difficult to obtain accurate displacement results. In such instances, the maximum displacement standard deviation along the riser length shown in Fig. 17 may be overpredicted since it will include participation from spurious higher and/or lower modes. An example is shown on the right of Fig. 5, where the displacements obtained from the modal analysis (solid lines) are larger than the displacements computed by

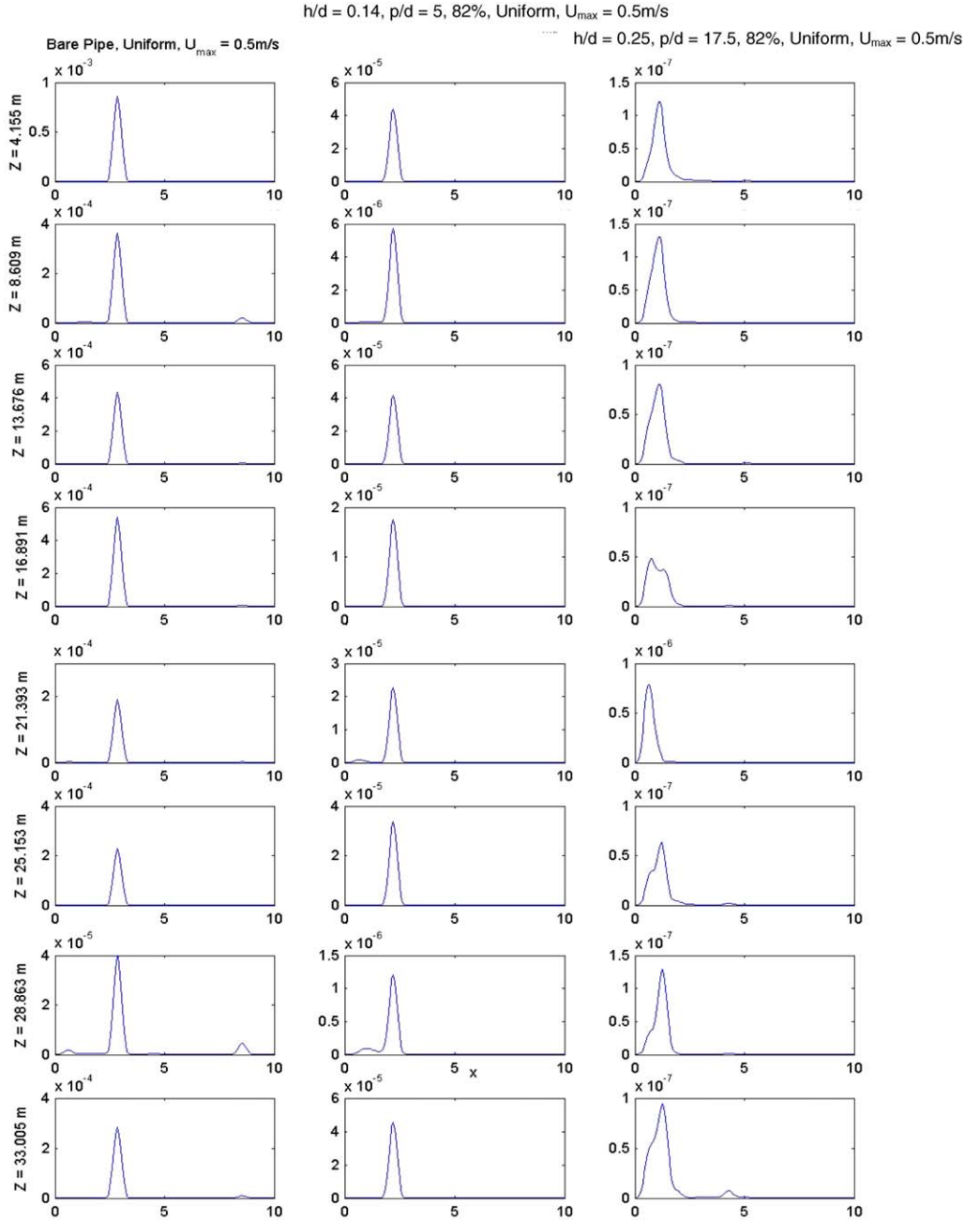

Fig. 9. Power spectral densities of CF displacement/diameter at different stations, Z, along riser in uniform flow. 0.5 m/s. Left column: bare riser. Centre column: 82% coverage of 5.0/0.14 strakes. Right column: 82% coverage of 17.5/0.25 strakes.

double integrating acceleration signals (hexagrams and diamonds). The mean values of displacement standard deviation are considered to be less sensitive to these errors.

Some asymmetry of the bare riser response in uniform flow is evident from Fig. 5, which may seem surprising. However, Marintek's experience is that some response asymmetry is always seen, even in highly symmetric test set-ups—possibly due to inherent unstable tendencies of fluid-structure interaction. The uneven spacing of gauges in the present tests may tend to promote any such instability, even though the total gauge coverage is very small (about 3.5%).

4.1. Bare riser response

Initially, a set of bare riser tests was performed to verify that high mode response could be obtained using this model and test rig and to provide benchmark fatigue damage calculations for the subsequent assessment of strake performance. In addition, these tests established whether the unsuppressed riser response followed trends typically

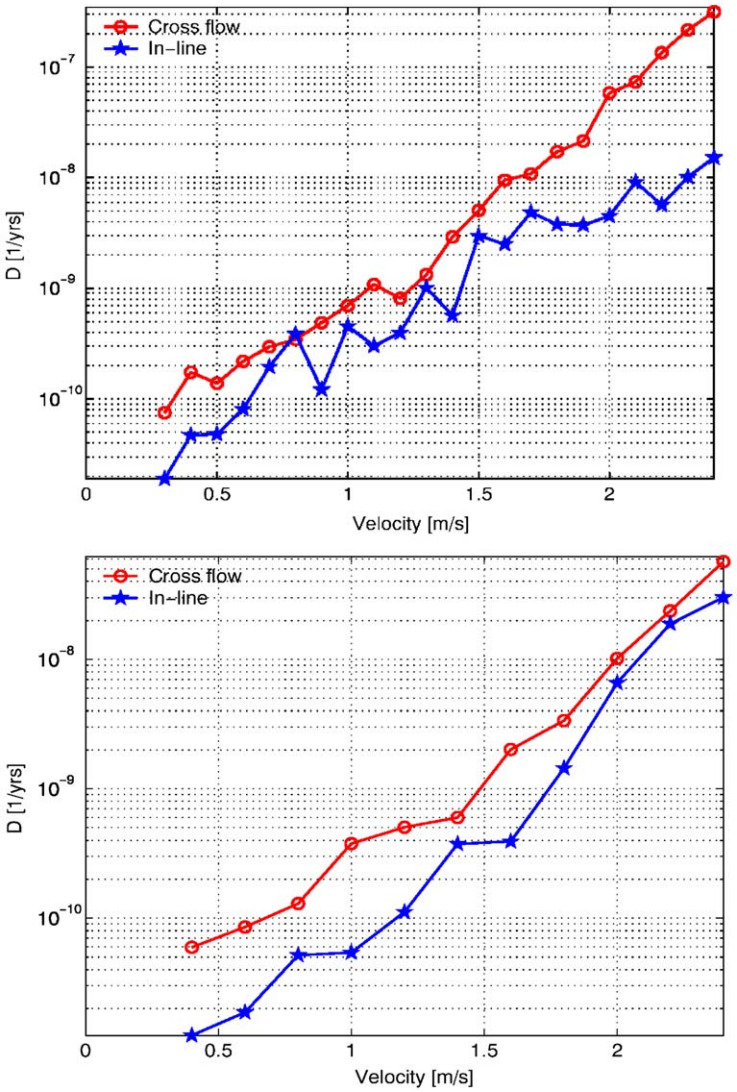

Fig. 10. Maximum CF and IL fatigue damage versus tow speed for 91% straked riser, 17.5/0.25. Top: uniform flow. Bottom: linearly sheared flow.

observed in previous flexible riser tests. The trends of interest were VIV response amplitude, frequency and modal behaviour.

4.1.1. VIV displacement amplitude

Figs. 16 and 17 present the mean and maximum of CF and IL displacement standard deviation for uniform and sheared flow. Bare riser results are shown in c1. Each pair of symbols (CF/IL) is representative of a single test. CF displacement is higher than IL displacement for all velocities. IL displacement is approximately $\frac{1}{3}$ of CF displacement. Generally, the uniform CF displacements are slightly higher than for sheared flow. Comparing Figs. 16 and 17, the trends with flow speed are similar. As a general rule, the standard deviations are approximately constant with respect to flow velocity for both CF and IL and are similar to results reported by Tognarelli et al. (2004) and Lie et al. (1997).

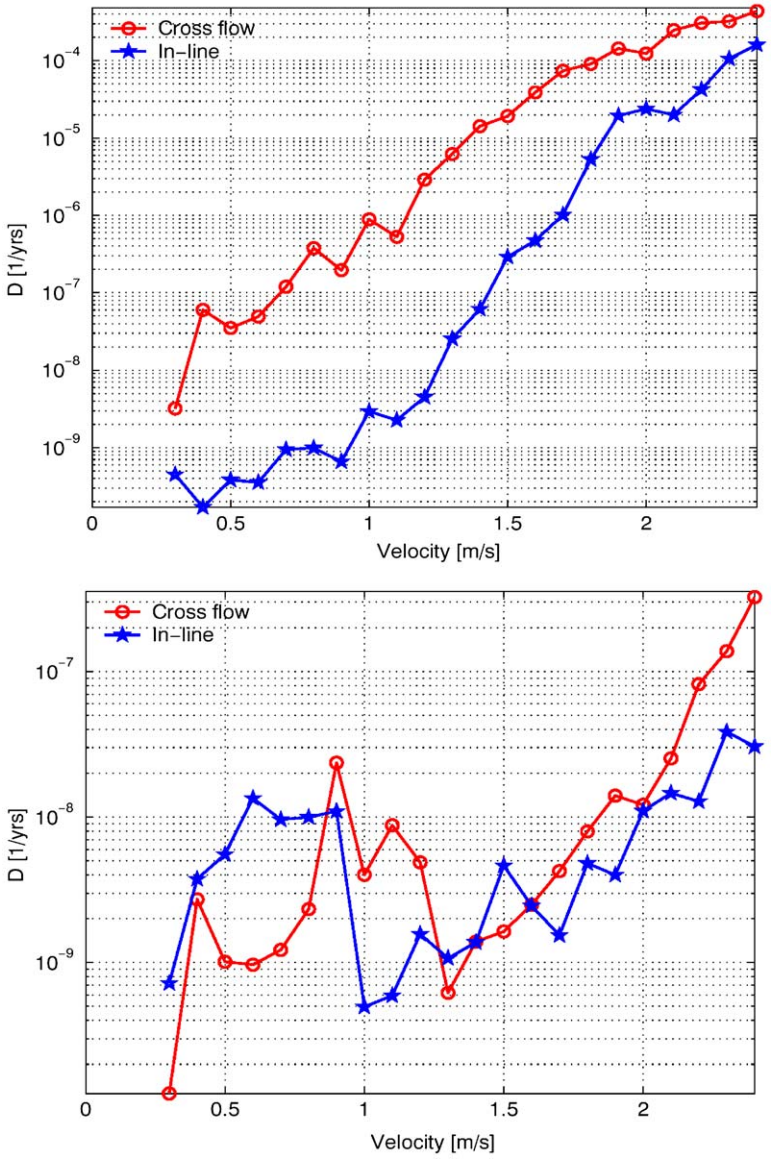

Fig. 11. Maximum CF and IL fatigue damage versus tow speed for 91% straked riser, 5.0/0.14. Top: uniform flow. Bottom: linearly sheared flow.

4.1.2. Response frequency

In Fig. 18, c1, the peak frequency of the dominant displacement mode is shown for the bare riser. For uniform flow (r1), the peak frequency of the CF dominant mode increases linearly with flow speed and is approximately half that of the IL dominant mode. For sheared flow (r3), the trends are similar. For reference, the shedding frequency is shown in each subplot for a stationary cylinder at low Reynolds number (Strouhal number = 0.2). It has been widely observed and reported that the response frequency of a vibrating cylinder will differ from the vortex-shedding frequency of a stationary cylinder. Similar phenomena are observed here.

4.1.3. Modal character

The dominant modes with respect to displacement and curvature are given in Figs. 19 and 20. Bare riser results are found in c1. Generally, the figures show increasing dominant mode number with increasing flow speed for both uniform and sheared flow. Consistent with the dominant frequency plots in Fig. 18, IL modes are approximately twice the CF modes. In Fig. 6 contour plots of the modal weight standard deviations for the bare riser in uniform and linearly sheared flow are presented. At low flow speeds there is a relatively narrow band of dominant modes in all cases. The band broadens out at higher flow speeds, most evidently for the CF response. The IL response in sheared flow exhibits the least broadening of all four cases, with a "gap" being apparent in the range 0.75–1.5 m/s—corresponding to a total response which stays roughly constant at a low level throughout this range (see Figs. 16 and 17).

4.1.4. Fatigue

Fig. 7 illustrates the maximum fatigue damage along the riser length as a function of tow speed in uniform and sheared flow for IL and CF directions. As reported by Tognarelli et al. (2004) and Baarholm et al. (2005), IL fatigue damage is about the same as CF fatigue damage. This is a very important observation considering that VIV analysis computer programs, to date, ignore the IL component of fatigue damage. It occurs due to the fact that, while IL displacement is less than CF displacement, the modal curvature and response frequency, which control fatigue damage, are much larger. Fatigue increases approximately in proportion to the seventh power of tow speed, which is expected for a riser with tension-dominated stiffness; see Baarholm et al. (2005). Similar trends are observed in uniform and linearly sheared flows, although the actual damage is less for the latter.

4.2. Fully straked riser response

This section shows that when the riser is fully covered with 17.5/0.25 strakes, VIV can be substantially mitigated in both uniform and linearly sheared flow. The results also show that a 5.0/0.14 strake geometry can reduce VIV response, though not as efficiently. This reduced efficiency has a very significant impact in terms of fatigue damage. Finally, the

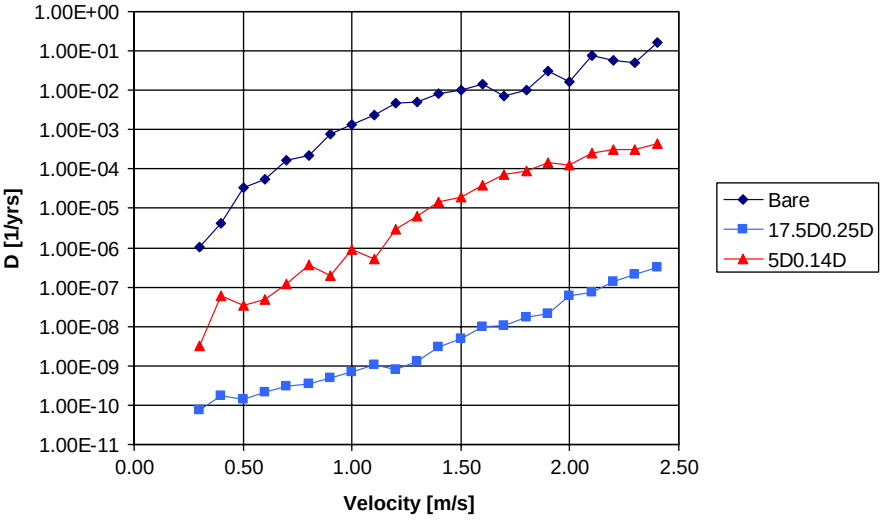

Fig. 12. Maximum CF fatigue damage in uniform flow for: bare riser, 91% coverage with 5.0/0.14 strakes, 91% coverage with 17.5/0.25 strakes.

results demonstrate that gaps in strake coverage due to practical considerations like banding and connections on full-scale risers have a negligible effect on strake performance.

4.2.1. VIV displacement amplitude

Compared to the bare riser, the displacements for the fully straked riser are significantly less, for both IL and CF directions. However, there are relatively large differences between the CF riser displacement standard deviations in uniform flow, depending on which strake geometry is utilized. The 5.0/0.14 strakes, Figs. 16 and 17, r2, c4 and c5, allow

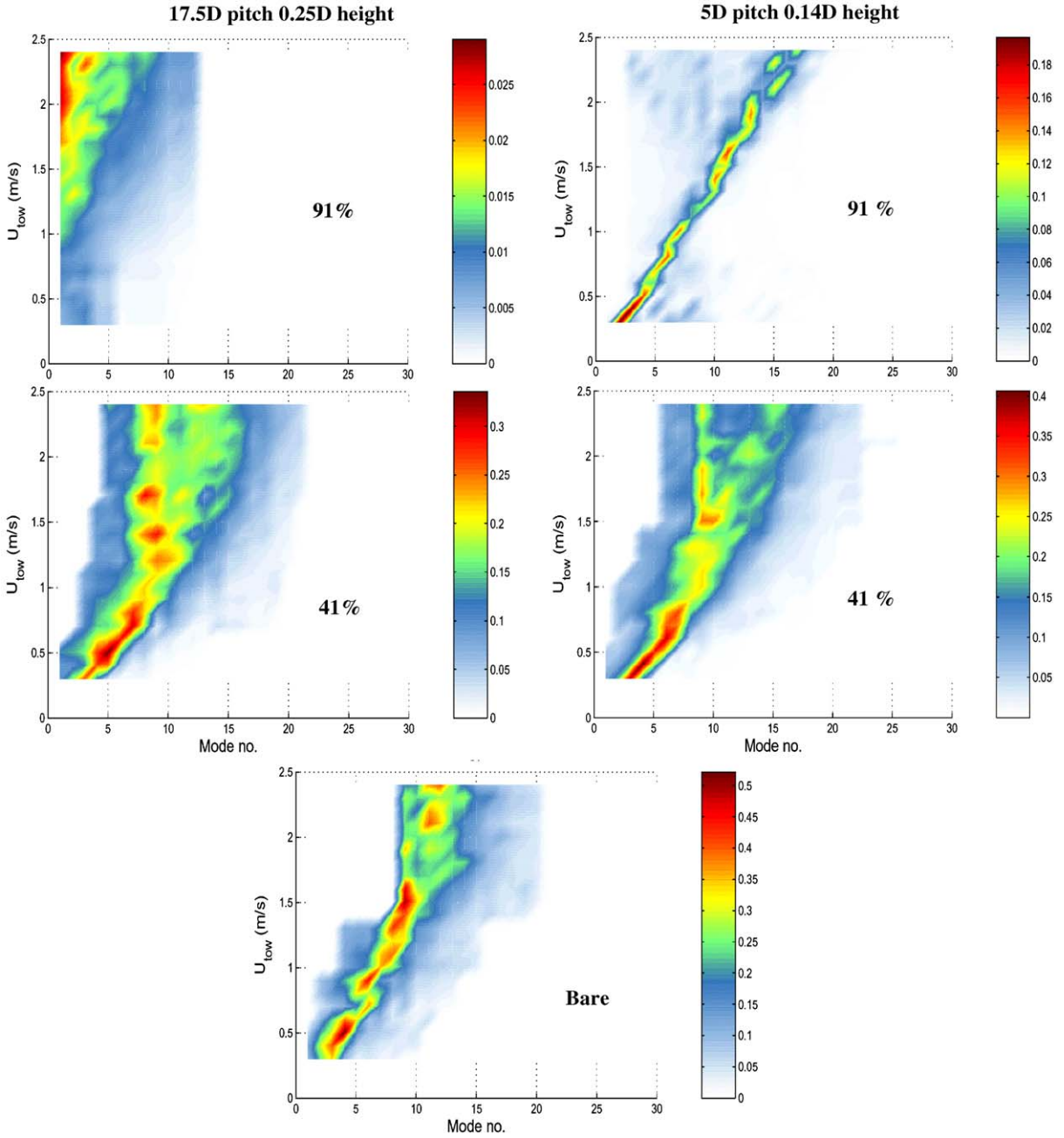

Fig. 13. Contour plot of CF displacement modal weight standard deviations in uniform flow. Left: 17.5/0.25 strakes. Right: 5.0/0.14 strakes. Top: 91% coverage. Middle: 41% coverage. Bottom: bare riser.

significantly larger displacements compared to the 17.5/0.25 strakes, r1, c4 and c5. This difference is compounded by the power law of the S–N curve when fatigue damage is calculated. The difference in performance of the strake geometries is not as noticeable in sheared current. However, it should be noted that both of the current profile shapes considered in these experiments are idealistic representations. Profiles in nature typically display some characteristics of both uniform and sheared shapes. Therefore, both sets of results are relevant for designers. Comparing the 4th and 5th columns of each row, it is apparent that breaks in the strake coverage for realistic cut-outs have very little impact on the response.

4.2.2. Response frequency

From Fig. 18, it can be seen that the response frequency for the riser fully covered with either strake geometry is quite different from the bare riser frequency response. The riser with the 17.5/0.25 strake profile responds at very low frequency in both uniform and sheared flow. The frequencies are nearly independent of tow speed and there is no clear relationship between IL and CF frequency. Frank et al. (2004) observed similar trends for a long riser model fully covered with strakes having 16D pitch and 0.25D height.

On the other hand, the response frequencies of the riser fully covered with the 5.0/0.14 strakes are strongly linear with tow speed in uniform flow. However, the IL and CF response frequencies are nearly identical in this case whereas they are separated by a factor of two when the riser is bare. This might suggest that some aspect of the VIV physical mechanism is more efficiently mitigated by the 17.5/0.25 strake geometry. In sheared flow, the riser response frequency when fully covered with 5.0/0.14 strakes also increases with tow speed, but the trend is much less distinct than in the uniform flow case.

Figs. 8 and 9 further illustrate fundamental differences between CF riser responses when fully covered with 17.5/0.25 strakes and when covered with 5.0/0.14 strakes. Fig. 8 shows time-traces of riser response (displacement/diameter) in uniform flow of 0.5 m/s. The displacements, in this case, were calculated by double-integrating the measured accelerations. Bare riser response is shown on the left, fully straked risers are shown in the centre (5.0/0.14) and at right (17.5/0.25). Notably, while the response is significantly reduced by the 5.0/0.14 strakes, it remains quite regular and much larger than the response when 17.5/0.25 strakes are used. The response with full coverage of 17.5/0.25 strakes appears more wide-banded. This is better illustrated in Fig. 9, which shows the power spectral densities that correspond to the time-traces in Fig. 8. Both the bare riser and 5.0/0.14-straked riser responses are generally narrow-banded in the vicinity of the stationary cylinder shedding frequency. The 17.5/0.25-straked riser response is more broad-banded and occurs at lower frequencies.

A possible benefit of the 5.0/0.14 strake is reduced drag due to its shorter height. Unfortunately, reliable IL drag measurements were not available from this experimental programme to assess this issue quantitatively.

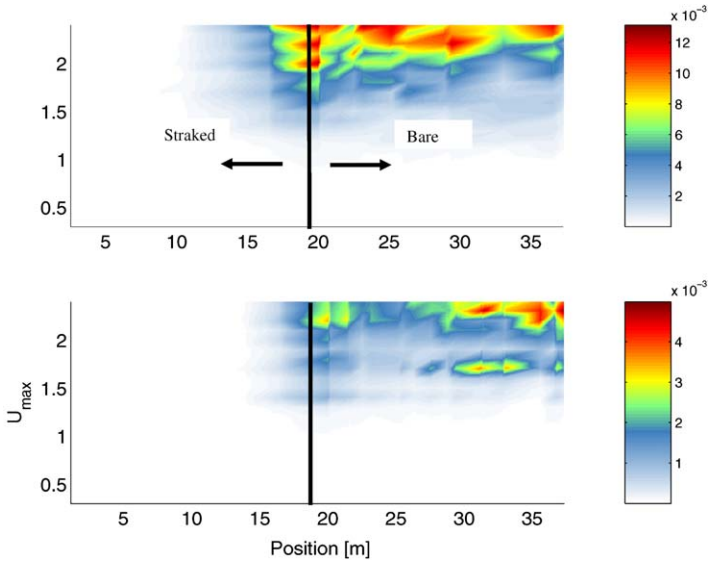

Fig. 14. Contour plot of local fatigue damage versus tow speed (m/s) for partially straked riser, 41% coverage with 17.5/0.25 strakes, uniform flow. Top: CF fatigue damage. Bottom: IL fatigue damage.

4.2.3. Modal character

The modal behaviour of the riser with strakes is also quite different from that of the bare riser, as seen from Figs. 19 and 20, c4 and c5. For the riser with the 17.5/0.25 strakes the dominant CF displacement mode is between 1 and 4 for both uniform and linearly sheared current profiles, r1 and r3, and is practically independent of tow speed. It is remarkable that the first mode is nearly always the dominant mode for IL displacement for both current profiles and in many cases is lower than the CF dominant mode.

For the riser fully covered with 5.0/0.14 strakes in uniform flow, r2, the dominant CF mode increases linearly with tow speed, similar to the bare riser response behaviour. For most cases the IL dominant mode is equal to the CF dominant mode, consistent with what was observed for dominant frequency. In sheared flow, r4, however, the dominant mode is generally lower and again independent of tow speed.

4.2.4. Fatigue

Since the displacements, dominant mode number and dominant frequency are all reduced by strakes, the computed fatigue damage is greatly reduced. Fig. 10 presents fatigue of the riser fully covered with 17.5/0.25 strakes. Comparison of Figs. 7 and 10 shows a reduction of five orders of magnitude in maximum fatigue damage when strakes are used in

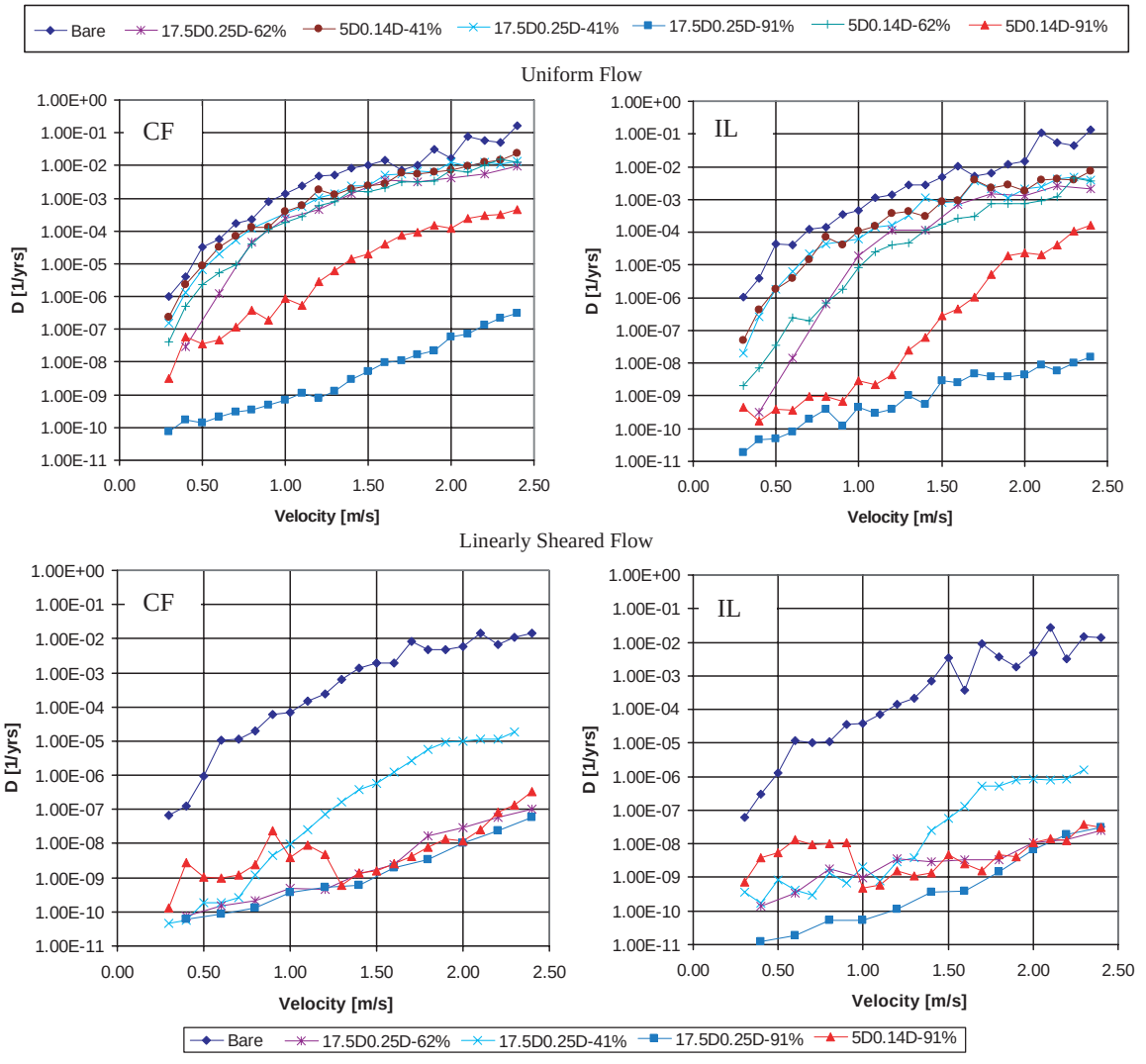

Fig. 15. Maximum fatigue damage versus tow speed for various suppression configurations.

Table 1
Descriptive summary of results

Coverage	Flow	Strake	Direction	Displ.	Frequency	Dominant mode	
						Displ.	Curv.
Bare	Uniform	None	CF	0.50	Linear (with flow speed)	3–12 S	2–12 S
			IL	0.15	Linear, twice CF	5–23 S	8–23 S
	Shear		CF	0.45	Linear	2–14 S	3–14 S
			IL	0.12	Linear, twice CF	4–25 S	4–25 S
Full	Uniform	17.5/0.25	CF	0.02	Very low	1–4 N	6–14 N
			IL	0.01	Very low	1 N	7–32 N
		5.0/0.14	CF	0.10	Linear	2–17S	3–17 S
			IL	0.02	Linear, same as CF	1–16 S	5–23 S
	Shear	17.5/0.25	CF	0.01	Very low	1–3 N	8–14 N
			IL	0.01	Very low	1 N	5–17 N
		5.0/0.14	CF	0.02	Low	1–6 N	3–14 N
			IL	0.02	Low	1–7 N	7–27 N
Partial	Uniform	17.5/0.25	CF	0.23	Linear	3–12 W	3–16 W
			IL	0.08	Linear, twice CF	4–20 W	5–25 W
		5.0/0.14	CF	0.30	Linear	3–15 W	3–18 S
			IL	0.06	Linear, same as or twice CF	4–22 W	5–25 S
	Shear	17.5/0.25	CF	0.08	Low/linear	1–9 W	2–12 W
			IL	0.01	Twice CF	1–13 W	5–16 W
		5.0/0.14	CF	—	—	—	—
			IL	—	—	—	—

uniform flow. A similar reduction is observed for linearly sheared flow. As a general rule, IL damage is somewhat less than CF damage, unlike the case of the bare riser.

Comparing Figs. 10 and 11, it can be seen that while the 5.0/0.14 strakes also reduce damage significantly compared to the bare riser case, they permit significantly more damage compared to the 17.5/0.25 strakes. For example, in uniform flow, the riser incurs up to 1000 times more damage when 5.0/0.14 strakes are used. A comparison of CF damage mitigation for the two strake geometries is shown for the 91% coverage case in Fig. 12.

4.3. Partially straked riser response

This section shows that the performance of helical strakes in suppressing VIV motions and damage is sensitive to the fraction of the riser's length covered. In particular, performance depends on current profile and the speed to which the bare section of riser is exposed.

4.3.1. VIV displacement amplitude

Figs. 16 and 17, r1 and r2, c2 and c3, show that in uniform flow, partial coverage of the riser with either strake geometry reduces displacement standard deviation somewhat, although the general trends with flow speed remain broadly the same as for the bare riser. This is true for both IL and CF response. Riser displacement with 62% coverage is appreciably less than with 41% coverage. That is, in general, increased strake coverage yields improved VIV mitigation.

Due to schedule constraints, only the 17.5/0.25 strake was tested in partial coverage in sheared flow; see Figs. 16 and 17, r3, c2 and c3. With 62% strake coverage, the displacements are almost as low as for the fully straked riser, but for 41% coverage they are significantly higher at higher flow speeds. This may be a reflection of the fact that in sheared current, the bare section of the riser is exposed to relatively low flow speeds compared to the straked section, with the maximum current speed experienced by the bare section increasing as strake coverage decreases.

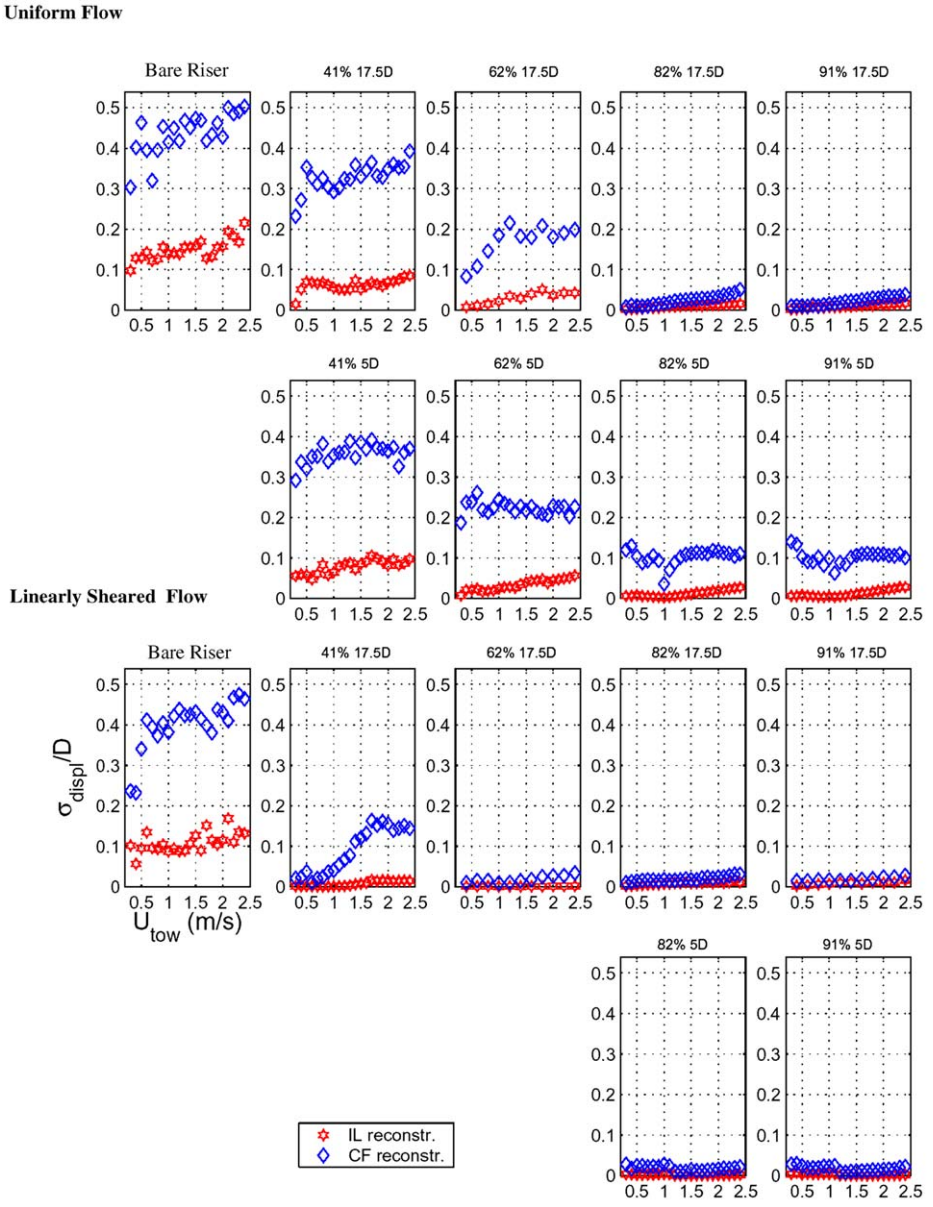

Fig. 16. Spatial mean of temporal displacement standard deviation for all tests.

4.3.2. Response frequency

The peak frequency of the dominant displacement mode for the partially straked riser is presented in Fig. 18, c2 and c3. For uniform flow, r1 and r2, the frequency of the CF dominant mode follows a linear trend for both strake geometries, similar to that for the bare riser. The IL frequency is in most cases twice the CF frequency, except for the case of 62% coverage with 5.0/0.14 strakes, where it is generally the same as the CF frequency.

For sheared flow (r3) the dominant frequencies in partial coverage tests are much smaller than those in uniform flow, although the IL frequency is again approximately twice the CF frequency. Recalling that in partially straked tests, coverage begins at the high-speed end, the maximum flow speed in the bare riser section will decrease in proportion to the coverage. If the bare section of riser dominates the VIV response, one would expect that the response frequency would be reduced in the same proportion. A close look at the responding frequencies (c2, r1 and r3) indicates a reduction of this kind.

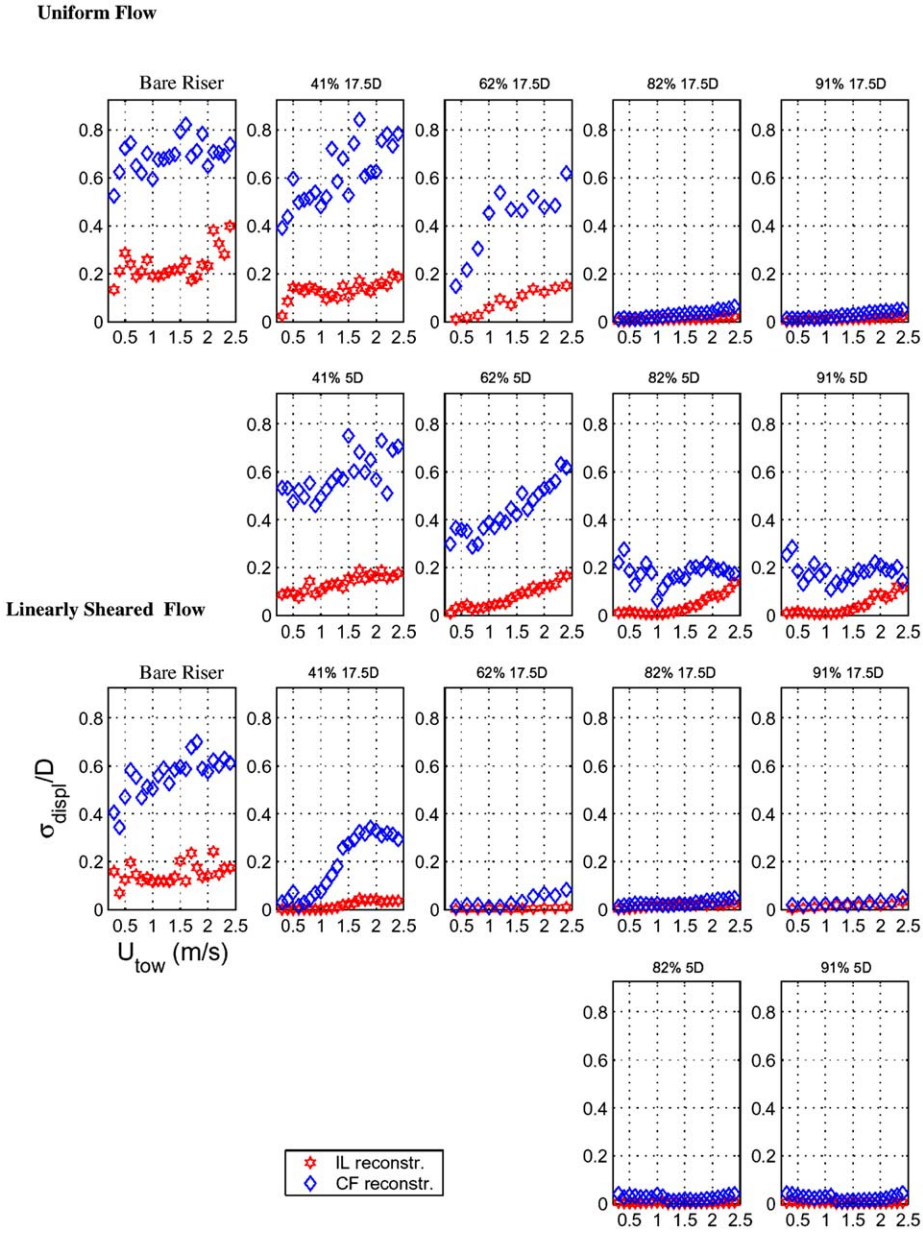

Fig. 17. Spatial maximum of temporal displacement standard deviation for all tests.

4.3.3. Modal character

Figs. 19 and 20, c2 and c3, show that in uniform flow, r1 and r2, the dominant mode trend when the riser is partially covered with either type of strake is similar to that for the bare riser. In sheared flow (r3) the riser with 62% coverage of 17.5/0.25 strakes behaves more like the fully straked riser, while the model with 41% coverage tends toward a bare riser response. This mixed response has been noted by Frank et al. (2004).

This is shown in more detail on the left of Fig. 13. The response with 41% coverage of 17.5/0.25 strakes is compared to a full coverage (91%) case and the bare, unsuppressed riser. Absolute modal participation factors decrease as strake coverage is increased and the trend transitions from linear to very low frequency.

The behaviour of the riser covered with 5.0/0.14 strakes is quite different, as shown on the right of Fig. 13. Again, the modal participation factors decrease as strake coverage is increased, indicating a dissipation of the total response. However, the linear trend of dominant mode with frequency appears to strengthen for a high-percentage coverage of

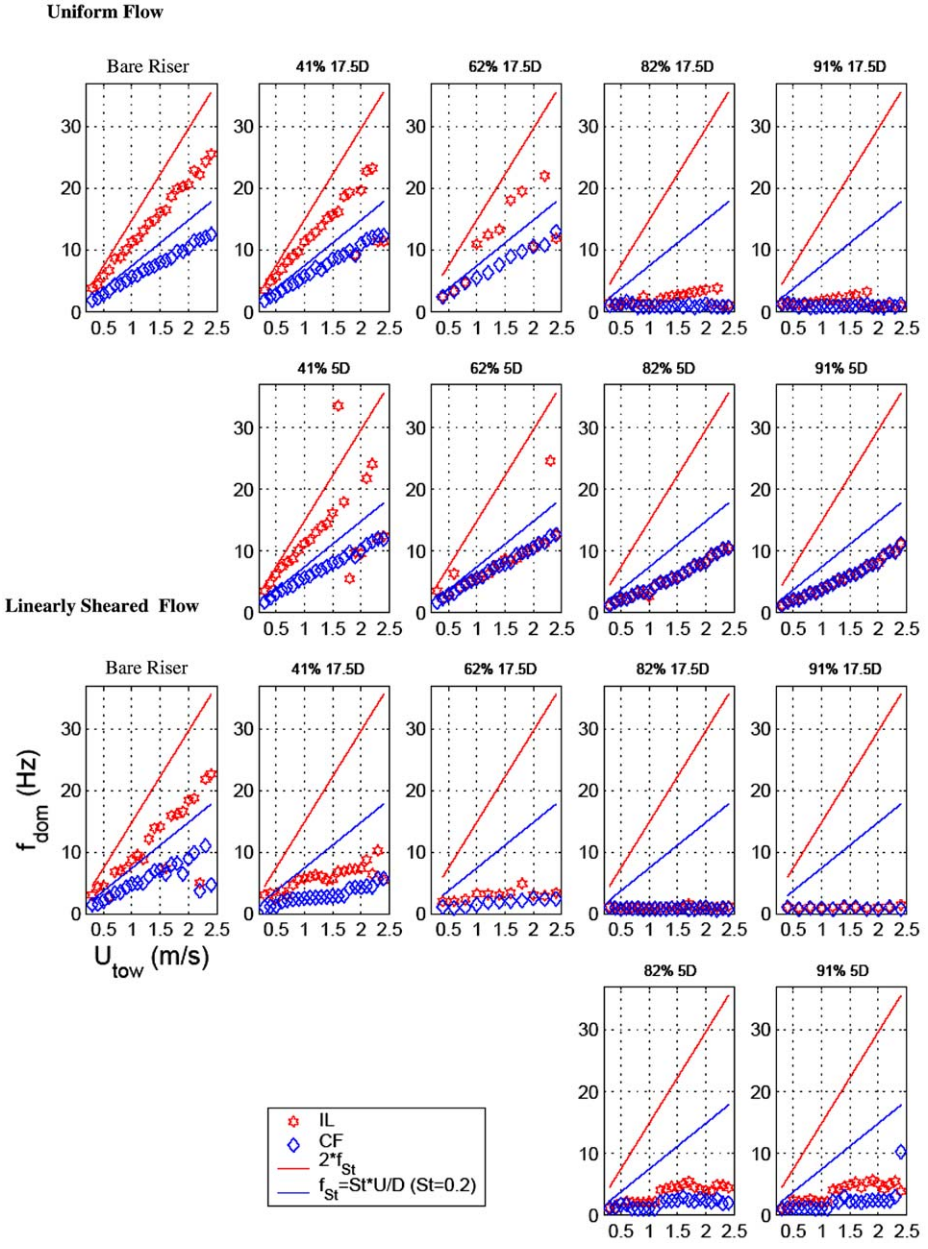

Fig. 18. Peak frequency of dominant displacement mode for all tests.

strakes. Finally, in general, modal participation factors are larger when 5.0/0.14 strakes are used as opposed to when 17.5/0.25 strakes are used, reflecting the decreased effectiveness of the 5.0/0.14 strakes in suppressing VIV.

4.3.4. *Fatigue*

Fig. 14 is a contour plot of fatigue damage along the 41% straked (17.5/0.25) riser in uniform flow. The left-hand side of the figure represents the portion of the riser that is covered with strakes. Although the maximum fatigue damage for the partially covered riser is significantly reduced compared to that of the unsuppressed riser (for this case a reduction in fatigue damage in the range 50–75%), there is a relatively large difference in local fatigue along the riser, with significantly less damage in the covered section compared to the bare section.

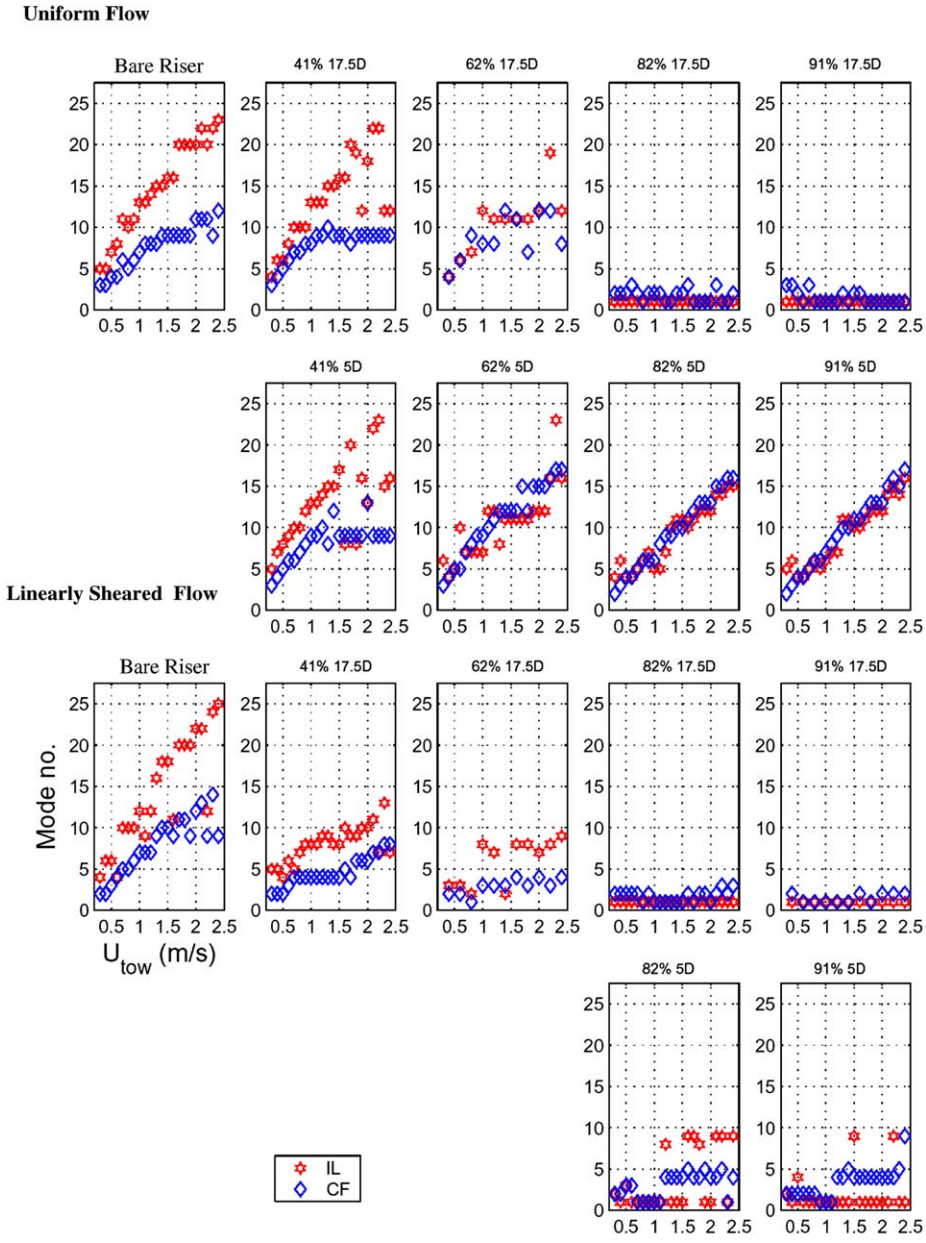

Fig. 19. Dominant mode with respect to displacement for all tests.

Fig. 15 shows a comparison of all strake coverages in mitigating damage in both current profile types. In uniform flow, particularly at higher velocities, it is evident that full coverage is required to significantly mitigate damage. In sheared flow, damage is mitigated by lower percentages of coverage because the strakes are always along the portion of the riser model where the current is highest.

4.4. Results summary

A descriptive summary of some of the key results presented and discussed above is given in Table 1. Note that values given in the displacement column are the mean of the standard deviations over the riser length. The response amplitude is scaled by the riser diameter. Maximum standard deviation follows similar trends and is shown in Fig. 17. In some cases detail has been sacrificed through the use of single numbers in Table 1 to represent what, more strictly, are

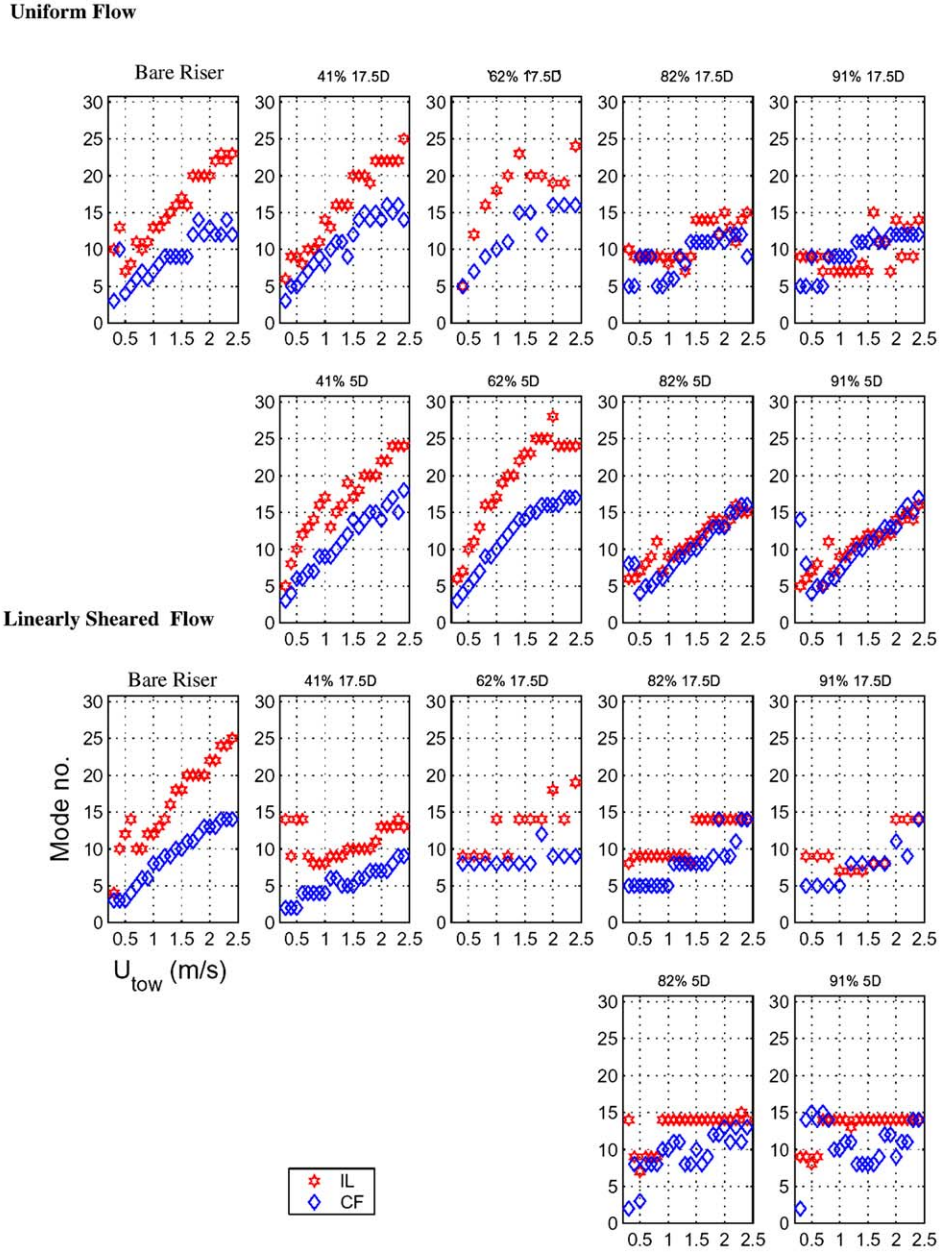

Fig. 20. Dominant mode with respect to curvature for all tests.

ranges—for the purpose of illustrating global trends. For finer detail, see Figs. 16–20. Riser diameter is taken as bare riser diameter in all cases, regardless of strake coverage.

For the dominant mode, the extent to which a clear trend follows flow speed is indicated by: S (strong), W (weak) or N (none), and there is some subjectivity in this categorization.

5. Conclusions

A model riser, 1400 diameters long, was tested in uniform and linearly sheared current profiles to determine VIV response. The bare riser was tested for benchmarking, and the performance of two strake geometries was then

evaluated. The geometries were: 17.5D pitch × 0.25D height and 5D pitch × 0.14D height—called 17.5/0.25 and 5.0/0.14, for convenience.

CF (cross-flow) and IL (in-line) responses were recorded in terms of spanwise strain and acceleration. Riser displacements were reconstructed by decomposing instantaneous strain and acceleration signals into structural modal contributions. Fatigue damage was calculated directly from the strain measurements.

As in some earlier studies, IL fatigue damage was observed to be of the same order as CF fatigue damage. This is very important to designers, since currently available VIV fatigue analysis programs do not include an IL contribution.

VIV displacement standard deviations of the bare riser in uniform and sheared flows were broadly consistent with findings which preceded the Marintek 2003 tests, although the IL displacement standard deviation was smaller than expected in sheared flow.

In sheared currents, both strake geometries were effective in suppressing VIV when a realistically attainable "full" coverage of 82% or more was used. In uniform flow, the 17.5/0.25 strake performed as well as it had in sheared flow, but the 5.0/0.14 strake was not as effective. Both designs of strake (82% coverage or more) suppressed IL VIV by almost 100% in sheared flow and about 90% (or more) in uniform flow in terms of strain.

As mentioned, fatigue damage rates CF and IL are of similar magnitude for the bare riser, but the IL damage decreases relative to the CF damage as strake coverage is increased. The "suppression" mentioned above refers to strain magnitude, but this suppression is generally accompanied by significant reductions in frequency, to which damage is linearly proportional. Additionally, in the calculation of fatigue damage an exponent of 3 or 4 typically applies to strain (or stress). Thus, the overall effect of strakes on fatigue damage is to reduce it by several orders of magnitude, rather than that which might be suggested by strain reduction alone.

Suppression performance may also be considered in the light of dominant mode number and associated frequency, both of which are reduced considerably when the riser is fully straked—with the exception of the 5.0/0.14 strake in uniform flow. It may be conjectured that this latter arrangement diminishes some aspect of the VIV physical mechanism for bare risers, but does not destroy it with the same effectiveness as the 17.5/0.25 strakes. According to similar reasoning as in the previous paragraph, the performance of the 5.0/0.14 strakes in uniform or uniform-like currents in mitigating damage could be expected to be significantly worse than that of the 17.5/0.25 strakes.

Reducing strake coverage from 91% to 82% to reflect practical limitations produces no significant change in the suppression performance for either design of strake. However, suppression effectiveness decays quite rapidly as the percentage coverage is further reduced. For partial coverage scenarios (where all strakes are grouped towards the end with the fastest flow) the response tends to be dominated by the highest shedding frequency from that part of the riser which remains bare. This implies that when partial coverage solutions are being considered, they should be accompanied by careful consideration of the flow field experienced by the exposed section of the riser.

Acknowledgments

The authors are grateful to NDP for permission to publish this paper. They would also like to thank Trygve Kristiansen and Gro Sagli Baarholm at MARINTEK for their enthusiastic and insightful analysis of the results.

References

Baarholm, G.S., Larsen, C.M., Lie, H., 2005. On fatigue damage accumulation from in-line and cross-flow vortex induced vibrations on risers. Journal of Fluids and Structures, in press, doi:10.1016/j.fluidstructs.2005.07.013.

Frank, W.R., Tognarelli, M.A., Slocum, S.T., Campbell, R.B., Balasubramanian, S., 2004. Flow-induced vibration of a long, flexible, straked cylinder in uniform and linearly sheared currents, OTC 16340, Offshore Technology Conference, Houston, Texas, USA.

Herfjord, K., Larsen, C.M., Furnes, G., Holmas, T., Randa, K., 1999. FSI-Simulation of vortex-induced vibrations of offshore structures, Conference on computational methods for fluid-structure interaction. Trondheim, Norway.

Kaasen, K.E., Lie, H., Solaas, F., Vandiver, J.K., 2000. Norwegian Deepwater Programme: Analysis of vortex-induced vibrations of marine risers based on full-scale measurements, OTC 11997, Offshore Technology Conference, Houston, Texas, USA.

Lie, H., Kaasen, K.E., 2005. Modal analysis of measures from a large-scale VIV model test of a riser in linearly sheared flow. Journal of Fluids and Structures, submitted for publication.

Lie, H., Larsen, C.M., Vandiver, J.K., 1997. Vortex induced vibrations of long marine risers; model test in a rotating rig. OMAE Conference, Vol. 1-B, Yokohama, Japan, pp. 241–252.

NORSOK Standard, 1998. Design of steel structures—annex C –fatigue strength analysis.

Tognarelli, M.A., Slocum, S.T., Frank, W.R., Campbell, R.B., 2004. VIV response of a long flexible cylinder in uniform and linearly sheared currents, OTC 16338, Offshore Technology Conference, Houston, Texas, USA.

Trim, A.D., Braaten, H., Lie, H., Herfjord, K., King, R., Makrygiannis, C.M., Meling, T.S., 2004. Experimental investigation of vortex-induced vibration of long marine risers, FIV2004 (Flow Induced Vibration) Conference, Ecole Polytechnique, Paris, France.

Vandiver, J.K., 1993. Dimensionless parameters important to the prediction of vortex-induced vibration of long, flexible cylinders in ocean currents. Journal of Fluids and Structures 7, 423–455.

Vandiver, J.K., Allen, D., Li, L., 1996. The occurrence of lock-in under highly sheared conditions. Journal of Fluids and Structures 10, 555–561.

Willden, R.H.J., Graham, J.M.R., 2001. Numerical prediction of VIV on long flexible circular cylinders. Journal of Fluids and Structures 15, 659–669.